Arch. Metall. Mater. **66** (2021), 2, 373-380

DOI: 10.24425/amm.2021.135868

Y. PALACI[1*], M. OLGUN[1]

INFLUENCES OF HEAT TREATMENT ON MECHANICAL BEHAVIOR AND MICROSTRUCTURE OF THE EXPLOSIVELY WELDED D GRADE STEEL / EN AW 5083 ALUMINIUM JOINT

In this study, the effects of heat treatment on aluminum/steel structural transition joint (STJ) strength were analyzed with ram tensile tests to find the right welding conditions. Before ram tensile tests, the specimens were subjected to different heat treatments to simulate possible thermal conditions, which may occur during the welding of STJ to the steel side of ship construction. Temperatures were varied from 100°C to 500°C, and durations were changed between 5-25 minutes in the heat treatments. The results of the ram tensile tests indicated that tensile strength decreased above 300°C. Micro-hardness test and microstructure examination were conducted to understand behavior change during ram tensile tests. The investigation showed that precipitation of the secondary hard phases with aging at interface above 300°C, reduced the bonding between aluminum and steel materials, which lead to a decrease of strength, and also changed the mechanical behavior of the STJ during ram test from ductile to brittle fracture. If the temperature is below 500°C and the duration is under 15 minutes, the STJ strength value meets the standard requirement. Short and rapid welding could be suggested to reduce heat buildup during welding.

Keywords: Triclad, Heat Treatment, Mechanical Properties, Dissimilar metal welding

1. Introduction

In recent years, aluminum constructions have been replacing steel constructions to reduce the weight of the structures in shipbuilding, automotive, and aerospace industries. When these two materials are needed to be used in the same structures, they are welded together by using STJ. Steel-aluminum STJ structures are manufactured by using explosive welding to keep temperature and duration as minimum as possible for the joining of the STJ layers without any flaw. However, during the welding of the steel side to STJ, temperature (1000°C) exceeds the melting temperature of the aluminum. Therefore, many different phases can be formed at the interface of the explosively welded aluminum and steel layers of the STJ, depending on the chemical composition of the layers. Costanza et al. [1] carried out mechanical tests and microstructure characterization of a clad made of ASTM A516 low carbon steel and A5086 aluminum. They found that hard precipitates nucleated at interface depending on the temperature and duration during the welding of steel sides of the joint. Shao et al. [2] observed hard precipitates as Fe_2Al_5 and $FeAl_3$ phases at the interface by the microprobe analysis at galvanized steel and aluminum-clad manufactured by arc welding. Zhang et al. [3] proved that the $FeAl_3$ phase precipitated from the Fe_2Al_5 phase based on their computational and empirical study. Nguyen and Huang [4] examined the A5052 aluminum alloy and SS400 steel joint. They claimed that, when the intermetallic layer is minimized, the butt joint quality is increased. Liu et al. [5] optimized hybrid laser arc welding parameters of Fe/Al STJ to reduce intermetallic phases and to prevent strength decrease. Sun et al. [6] reached 120 MPa tensile strength at Al-Fe butt joints by fiber laser welding with precise temperature control of the interface. Meco et al. [7] developed a finite element (FE) thermal model by varying the interaction time and power density to calculate the transient heat treatment at the Fe-Al interface to maximize strength. Tricarico and Spina [8] investigated the influences of the laser-induced thermal loads on the Fe/Al bond interface. Phengsakula and Rodchanarowana [9] investigated the amount of precipitation phase in aluminum 5083 layers of Fe/Al joint, which was remarkably raised after 5 and 15 minutes of thermal treatment at 300°C. Tricarico and Spina [10] showed that thermal loads did not affect strength at temperatures below 300°C. Tricarico and Spina [11] also studied impacts of the heat treatments on joint properties during laser welding.

Sun et al. [12] examined the straight and wave shape bond of explosive welded Fe/Al clad tube. Similarly, Paul et al. [13] showed the existence of flat and wavy interfaces in explosive

[1] YILDIZ TECHNICAL UNIVERSITY, NAVAL ARCH. AND MARINE ENG. DEPT, BESIKTAS, ISTANBUL, TR

* Corresponding Author: y_palaci@yahoo.com

welded Al/Cu and Ti/Ni interfaces. At the front slope of the waves, interface regions were locally melted and fluctuated the chemical composition. Paul et al. [14] investigated the heat transfer effect on the microstructural and chemical composition changes during explosive welding and annealing of those STJ's; Cu/Al, Ti/Al, stainless steel/Ta, stainless steel/Zr, and carbon steel/Ti. Hasenclever [15] investigated the effect of intermediate annealing on the strength of Al-Fe-alloys (AA1050-8021). He pointed out that annealing is vital for recovery behavior; the tensile strength was decreased from 200 MPa to below 100 MPa with increasing annealing temperature. Jimenez-Mena et al. [16] examined the nature of the intermetallic layer and control of the thickness to improve weld toughness by the addition of nickel or cobalt by electroplating. Shiran et al. [17] investigated the effects of stand-off distance on the interfacial metallurgical and mechanical specifications of explosively bonded 321 austenitic stainless steel to 1230 aluminum alloys by using a scanning electron microscope, optical microscopy, and microhardness test. Agudo et al. [18] examined interface microstructure between zinc coated ferritic steel and Al-alloy sheet joined by a cold metal transfer method by using transmission and scanning electron microscopy. They claimed that Fe_2Al_5 grains grew from steel sides, and $FeAl_3$ grains grew through Al sides. Springer et al. [19] investigated the effect of Zn on the intermetallic phase formation and growth when coated on steel before solid-state welding with aluminum by experiments and simulations. It was asserted that the Zn coating caused a detrimental effect on welding. However, Ca, Si, Sr, and Mg element addition to Al alloys led to better weldability. Matysik et al. [20] presented the effects of processing parameters and aluminum content on phase composition. In their investigation, chemical composition, phase transformations, and mechanical properties of $FeAl_2$, Fe_2Al_5, and $FeAl_3$ structures were studied by using SEM and EDS. The obtained results were verified with XRD, and the hardness of the phases was measured by using the nano-indentation technique.

For shipbuilding structural transition joint application, explosively welded joint material composed of D Grade Steel, 5083 series aluminum, and 1050 series aluminum as the intermediate layer is commonly used and well known available STJ. However, there is no detailed study relating to shipbuilding D Grade Steel STJ. Therefore, this study was performed to figure out the critical temperature and duration for this STJ. A decrease in the STJ strength and intermetallic layers has been examined relating to thermal effect. In addition, micro-hardness values were measured at the interface to understand the relation between hardness and thermal effect. Finally, thermal effects on all examined properties were analyzed all together to understand limitations must be taken into consideration during the welding of the STJ steel side.

2. Materials and Method

In this study, the structural transition joint purchased from the Merrem & La Porte Company, with the trade name "Triclad" was used. Mechanical properties and chemical contents of the STJ layers were given in Table 1, and Table 2 obtained from the certificates presented by the vendor company. Triclad is a combination of 3 layers, which are shipbuilding steel LR grade D steel as bottom plate, 5083 aluminum alloy (AA5083) as top plate, and 1050 aluminum alloy (AA1050) as an intermediate layer. The thicknesses of each STJ layer are given in Table 2.

TABLE 1

Alloying element contents of STJ (Triclad) produced by the Merrem & La Porte Company

Elements (at.-%)	Shipbuilding Grade D	Aluminum 1050	Aluminum 5083
C	0.103		
Al	0,038	99.609	94.246
Mn	1.085	0.012	0.560
P	0.014		
S	0.003		
Si	0.199	0.040	0.190
Fe	98.566	0.320	0.350
Cu	0.013	0.002	0.031
Mg			4.490
Zn		0.004	0.018
Ti		0.013	0.015
Cr	0.017		0.100

TABLE 2

Triclad layers and their mechanical properties

Properties	Shipbuilding Grade D (15 mm)	Aluminum 1050 (3 mm)	Aluminum 5083 (10 mm)
Tensile Strength (MPa)	420	132	297
Yield Strength (MPa)	318	123	163
Elongation (%)	36.5	9	25

Ten specimens were machined to perform ram tensile tests according to the MIL-J-24445A standard that explains the test set up to measure the strength of the steel-aluminum interface. Different heat treatments were applied to the specimens before starting the ram tensile test to understand the effect of revealed heat during welding on interface strength. As an exception, specimens 1 and 2 were tested with their initial state as a received condition without any heat treatment. The heat treatment is carried out according to the conditions given in Table 3. During heat treatment, the furnace first heated to a given temperature, and then the specimens were put into the hot furnace and stayed there for a given duration. When the specified duration reached, the specimens were taken out of furnace and air-cooled at ambient temperature.

Additional ten specimens were prepared for microstructure and microhardness tests. The samples were polished before hardness measurements and microstructure inspections. Surface preparation of the specimens consisted of grinding trough 1200-grit emery papers and then polishing was completed by using diamond paste having 6 μm and 1 μm average particle

TABLE 3

The heat treatment conditions and the ram tensile test results

Specimen No.	Temperature (°C)	Time (min.)	Tensile Strength (MPa)
1	as received		202.4
2	as received		199.4
3	300	5	196.8
4	300	15	183.8
5	300	25	185.2
6	400	15	171.9
7	400	20	151.9
8	500	5	196.7
9	500	15	117.0
10	500	25	71.0

sizes, respectively. Steel sides of the specimens were chemically etched with Nital solution (5 mL HNO_3 and 190 mL H_2O) for 15 seconds, and aluminum sides of the samples were etched with Keller reagent (2 mL HNO_3 and 98 mL C_2H_5OH) for 10 seconds to make the intermetallic phases and particle structures more apparent.

2.1. The ram tensile tests

The ram tensile tests were carried out by using a tensile test machine purchased from Alsa Company. During the testing process, the punch speed was 0.05 mm/s, and the pre-load force was 30 N/mm^2. While the punch was in contact with the test sample, the specimen was loaded until it failed. The maximum stress values were recorded during the experiment to evaluate the joint strength for different temperature-time cycles. For each test, force-displacement data were recorded in real-time.

2.2. Microstructure Investigations

The microstructure analysis of the heat-treated transition joint samples was performed with the Scanning Electron Microscope (SEM) ZEISS EVO LS 10 instrument. SEM analyzes were achieved by visually controlling the morphology of the Fe/Al interface and taking quantitative EDS analysis from selected locations. For the hardness and microstructure investigations, specimens 2, 5, and 10 were selected. These three specimens had one moderate and two extreme strength values during ram tensile tests, as seen in Table 3. In the selected samples, the first sample had no heat treatment, and the other two samples had the same holding time with different temperatures as 300°C and 500°C.

2.3. Microhardness tests

These tests were carried out to measure the hardness of the Fe/Al interface by taking hardness values at different locations to analyze phases. The investigations were carried out by using an HVS-1000 Digital Micro Vickers Hardness Tester. During measurements, the load was set to 500 grams for 10 seconds, and five measurements were taken at specific locations, near the Fe/Al interface and far away from the Fe/Al interface for each sample. Determined measurement locations and their distances from the interface are shown in Fig. 1.

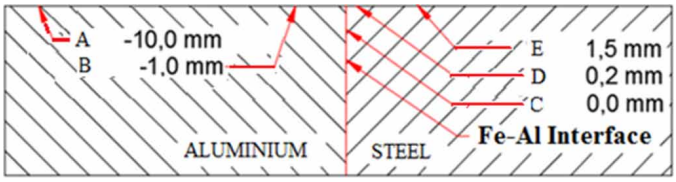

Fig. 1. Hardness measurement locations

Three measurements were taken from each selected point, and the mean values of three measures were taken as hardness value. Table 3 shows the heat treatment conditions of each specimen prepared for microhardness and microstructure investigations. Specimen 10 (500°C, 25 min.) represents the heat-treated sample at the near-melting point of aluminum, while specimen 2 (as received) represents the transition joint that was not exposed to any heat treatment.

2.4. XRD Analysis

XRD analysis was performed to identify crystal phases on the ram test specimens' fractured both surfaces by the Panalytical expert XRD diffractometer. ICDD (international diffraction center) software was used in the phase definitions. Quantitative phase analyzes were calculated in the analysis program using the Rietveld method. 2θ was scanned using Cu-Ka1 (1.5406 Å) radiation in the range of 20 to 120 degrees.

3. Results and discussion

In this study, ram tensile tests, micro-hardness tests, and microstructure examinations of heat-treated TRICLAD were performed to understand the temperature and time limits in which STJ owns the required strength. Heat treatments were carried out at different temperatures ranging from 300°C to 500°C and different durations such as 5, 15, and 25 minutes.

The results of ram tensile tests are presented in Table 3, and Fig. 2 shows changes in tensile strength up to 500°C for certain exposure times. As seen in Fig. 2, when the exposure time is 5 minutes, there is no significant change in strength with temperature increase in the studied range. The tensile strength values of all specimens were very close to 200 MPa. When the exposure time increased to 15 minutes, the tensile strength decreased to 117 MPa at 500°C. Nevertheless, it is still above the limit value required by the standard (75 MPa). At 25 minutes of holding time, strength decreased significantly with temperature change.

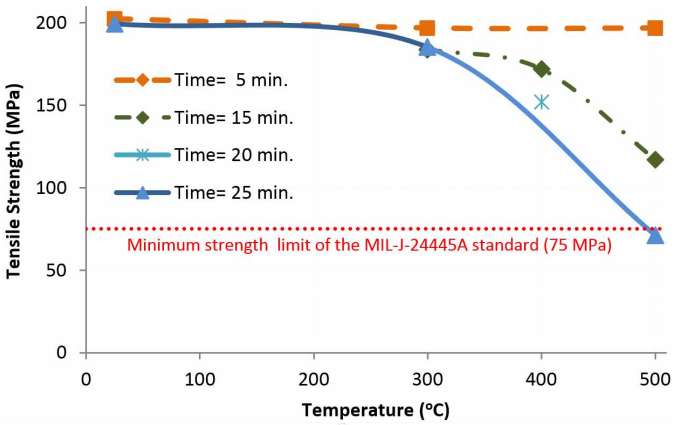

Fig. 2. Tensile strength of specimens according to heat treatment temperature and duration

It went below the limit value required by the standard when the temperature raised to 500°C. The same trend has been observed in other studies [8,10,11]. Therefore, excessive and thick welding must be avoided. A short and rapid welding method must be preferred instead of continuous long welding. When the temperature is kept below 500°C and exposure time is less than 15 minutes, it is possible to prepare welding with the required STJ strength. Measured tensile strength values in the current study are very close to values in the above referenced studies. Although steels were different from each other, intermediate layers (AA1050) are the same for all compared studies, and they are the weakest layer of the STJs. Similarly, highly deformed AA1050 tensile strength decreased to 86 MPa from 149 MPa when annealed at 350°C for 10 min. [21]. We should keep in mind this event also when we consider STJ strength.

Back-scattered electron (BSE) images of microstructure and SEM-EDS analysis near the Fe/Al interface in specimen 2 are given in Fig. 3. The black area shows AA1050 pure aluminum section, a light gray area demonstrates the Shipbuilding Grade D steel section, and the dark gray section is the diffusion zone at the interface where steel and aluminum atoms formed intermetallic phases. As can be seen in Fig. 3, Spot-1 shows nearly 67.2 at.% Al content at the spot locations in the dark gray section at the interface of the specimen 2. Specimen 5 and specimen 10 inter-

Locations	SEM EDS analysis (at.-%).		
	Al K	Fe K	Mn K
Spot 1	67.2	32.8	
Spot 2	100.0	0	
Spot 3		98.3	1.7

Fig. 3. Back-scattered electron (BSE) image of Specimen 2 (as received)

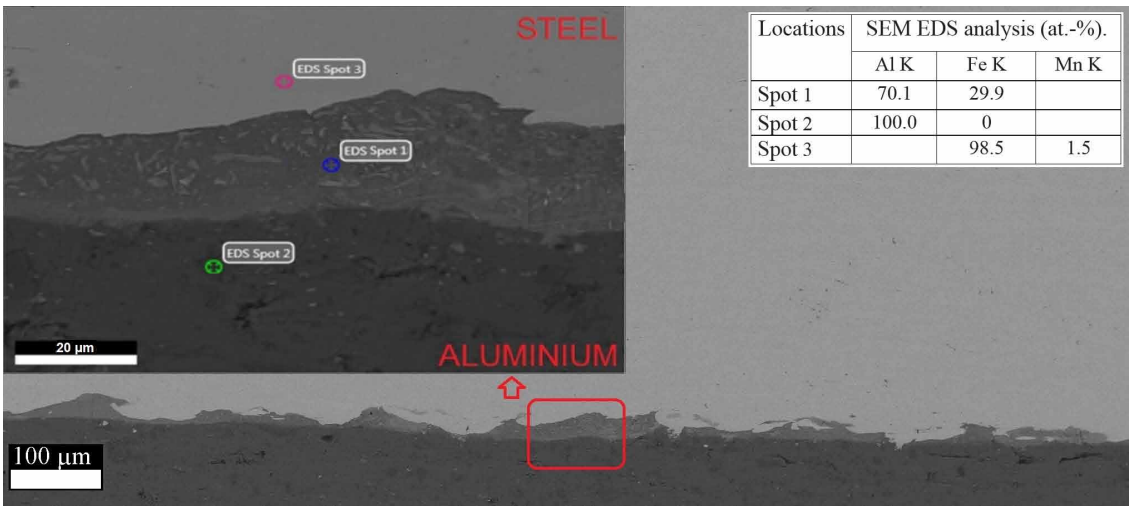

Locations	SEM EDS analysis (at.-%).		
	Al K	Fe K	Mn K
Spot 1	70.1	29.9	
Spot 2	100.0	0	
Spot 3		98.5	1.5

Fig. 4. Back-scattered electron (BSE) image of Specimen 5 (300°C, 25 min.)

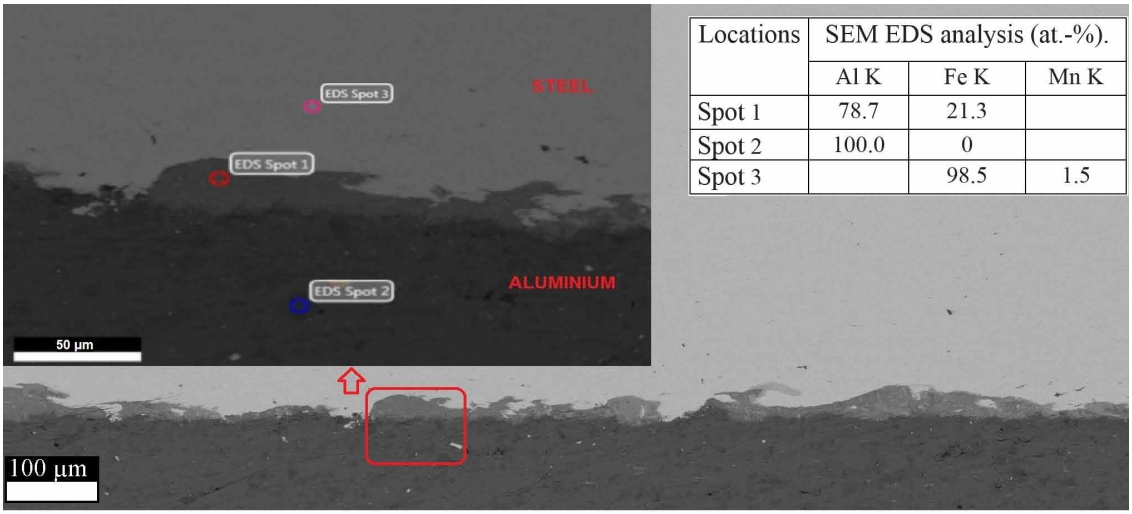

Locations	SEM EDS analysis (at.-%).		
	Al K	Fe K	Mn K
Spot 1	78.7	21.3	
Spot 2	100.0	0	
Spot 3		98.5	1.5

Fig. 5. Back-scattered electron (BSE) image of Specimen 10 (500°C, 25 min.)

face region BSE images are shown in Fig. 4 and Fig. 5. As can be seen from the figures, Spot-1 shows nearly 70.1 and 78.7 at.% Al content in the dark gray diffusion zone of the specimen 5 and specimen 10 interfaces, respectively. As expected, 100 at.% Al was observed at Spot 2 locations of all specimens. Aluminum atom concentration raised by an increase in temperature and time, which enhanced diffusion of aluminum atoms and the formation of intermetallics like $FeAl_6$ and Fe_2Al_5, as seen in Table 4. Similarly, the formation of the intermetallics could be observed by the increase in the hardness value of the interface given in Table 5.

Fig. 3 shows a flat bonding interface of specimen 2 with the island of the intermetallics with the nearly 20 µm thickness or height and 100-150 µm length. It is challenging to consider interface as a wavy structure. The intermetallic structure is discontinued and irregular in between the Al-Fe interface. When specimen 5 (Fig. 4) and specimen 10 (Fig. 5) are studied, their interface macro view has less discontinuity and nearly two times more thickness compared to specimen 2. An increase in temperature enhanced intermetallic growth and reduced Al-Fe bonding by Al diffusion through the steel side.

Intermetallic phases were analyzed with XRD to investigate the phase transformations with heat treatment on the fractured surface from two sides (aluminum and steel). XRD pattern is given in Fig. 6, and detected intermetallic phases were summarized in Table 4. As seen from Table 4, Fe_2Al_5 phase at the steel side and $FeAl_6$ metastable phase exist only in specimen 10 aluminium side, and Al diffused to form or transform into these Al-rich phases at 500°C for 25 min. duration. The nucleation of metastable phases during fast cooling is expected [22]. When the amount of Al increased, the more brittle phases are formed. According to the literature, different intermetallic phases have different hardness values. It is pointed out that a sequence was observed as follows in terms of hardness: Fe_2Al_5 (9.5-11 GPa-HV) > FeAl (4-5.2 GPa-HV) > Fe_3Al (2.5-3.5 GPa-HV) [20] There is no data in the literature relating to mechanical properties of metastable intermetallic phase $FeAl_6$ detected on the fracture surface of specimen 10 aluminium side in XRD analysis. This

TABLE 4

Fractured ram specimen XRD analysis of intermetallic phases from two sides

Existing Phases	Specimen 2 fractured side		Specimen 5 fractured side		Specimen 10 fractured side	
	Aluminium	Steel	Aluminium	Steel	Aluminium	Steel
Fe_3Al	√	√	√	√	√	√
FeAl	√	√	√	√	√	√
$FeAl_6$					√	
Fe_2Al_5	√		√		√	√

TABLE 5

Hardness values (HV) taken near steel-aluminium interface of the selected specimens

Heat treatment condition	Specimen No	Location A 10.00 mm	Location B 1.00 mm	Location C 0 mm	Location D –0.2 mm	Location E –1.5 mm
As received	2	90.3	38.0	220.8	204.7	187.7
300 °C/25 min.	5	86.0	43.3	237.0	193.3	188.0
500 °C/25 min.	10	91.0	53.3	280.0	221.3	192.3

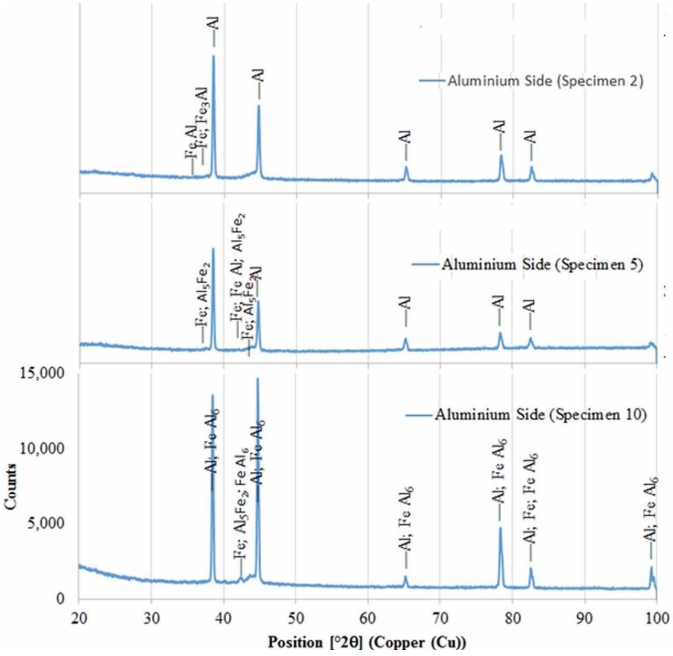

Fig. 6. XRD Analysis of the aluminum side of the specimens' fracture surfaces after ram tests

indicates fracture along $FeAl_6$ metastable phase during failure of the ram specimen under tensile load.

As can be seen from Fig. 7, the upper sides of the pictures represent the steel side of STJ specimens' fracture surfaces, and others represent the aluminum side. If the cross-sectional view of the specimen is examined in Fig. 7, two different types of interface could be noticed on the ram test sample. The interface between AA1050 intermediate aluminum layer and AA5083 aluminum layer has a regular wavy shape with a nearly 1.5 mm wave height and 5.5 mm wavelength. However, the interface between AA1050 and the steel layer has a flat shape bonding. When we examine a magnified picture of a location in the fracture surfaces of the steel side given in Fig. 8, wavy shape in the black and white color region can be noticed. The black color areas belong to the deformed tear region of the aluminum-rich soft layer. The sharp upright tips perpendicular to the specimen surface are visible ductile fracture images of samples subjected tensile loads. On the other hand, white regions have fragmented brittle fractures, with many small pieces lying parallel to the specimen surface. Even the deformed wavy black surface of specimen 2 and 10 can be seen in more detail in Figs. 9 and 10. The increase in temperature and time resulted in intermetallic layer growth, and more brittle failure agreed with ref. [10]. Fig. 11 shows Spectrum 1 region where SEM-EDS analysis was performed on the fracture surface of the specimen 2. The black region analyzed has a high aluminum content. Spectrum 2 in the white region shows intermetallic phases with higher Fe content as same as the spectrums of specimen 10. The weakest link in the chain is the intermediate soft AA1050 material of STJ, and it will fail first during ram test. The increase in temperature and time resulted in intermetallic layer growth and minimization of

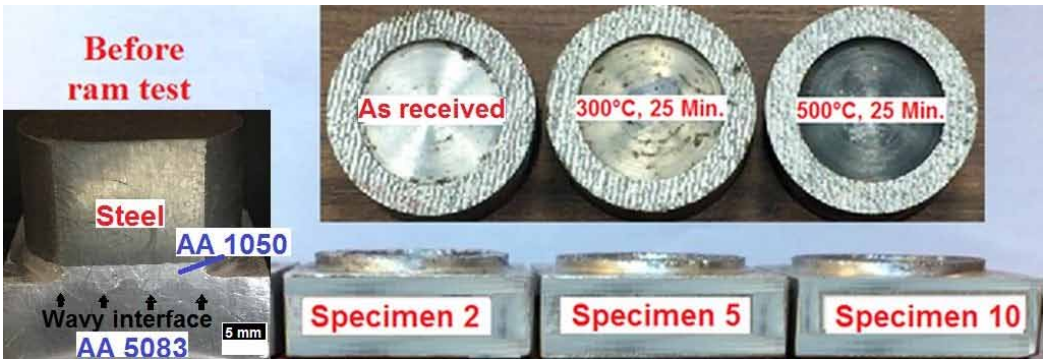

Fig. 7. Interface side view before ram test and fracture surfaces of the specimens after ram tests

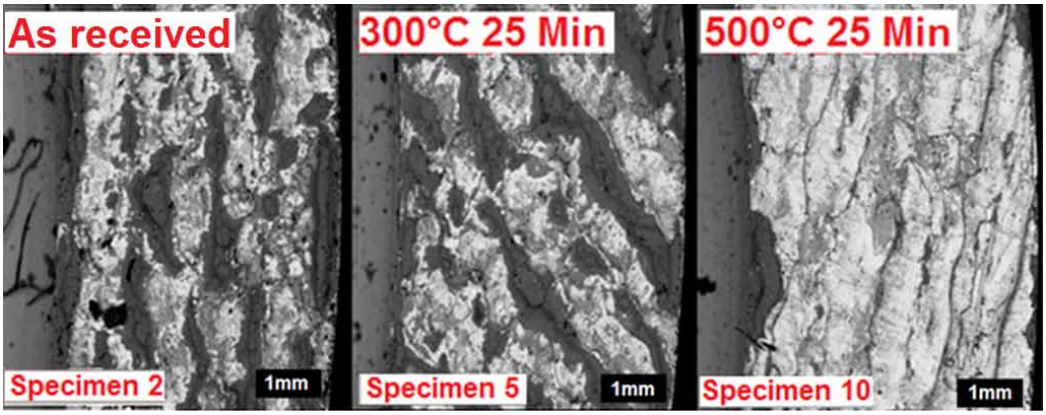

Fig. 8. SEM pictures of fracture surfaces of the specimens after ram tests

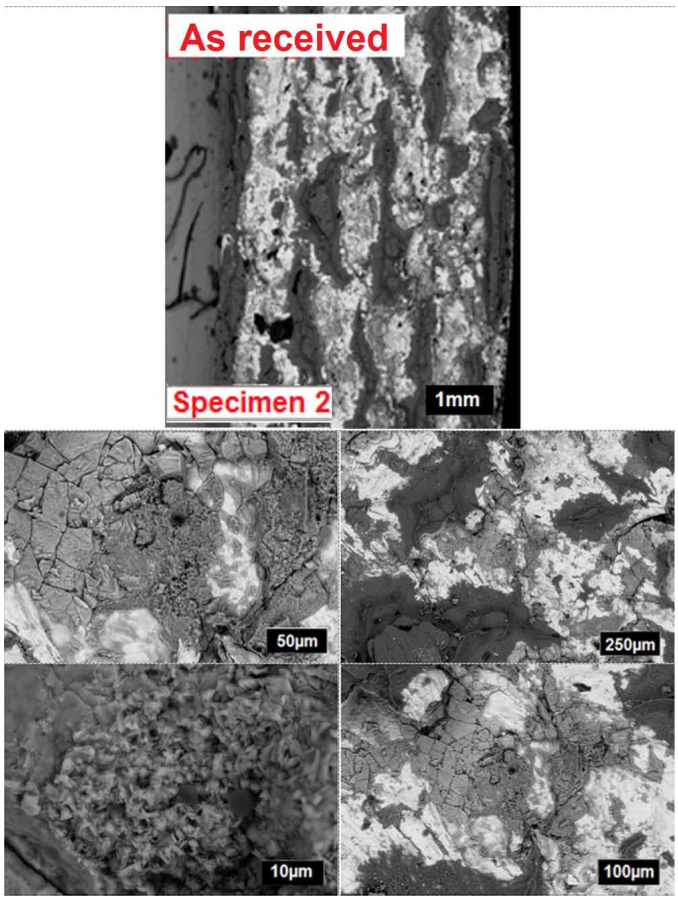

Fig. 9. SEM pictures of the fracture surfaces of specimen 2 after ram tests

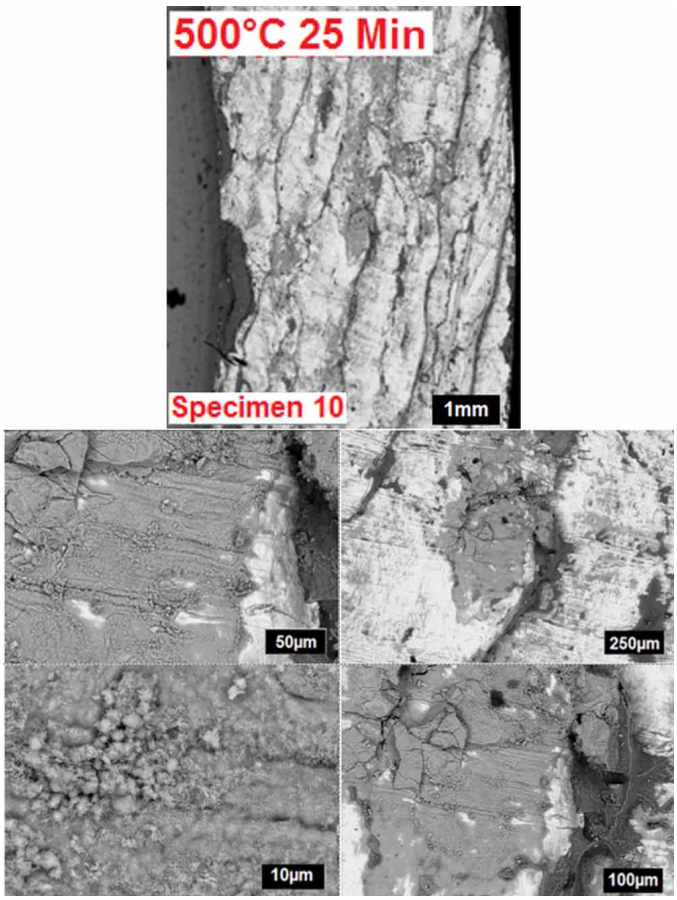

Fig. 10. SEM pictures of the fracture surfaces of specimen 10 after ram tests

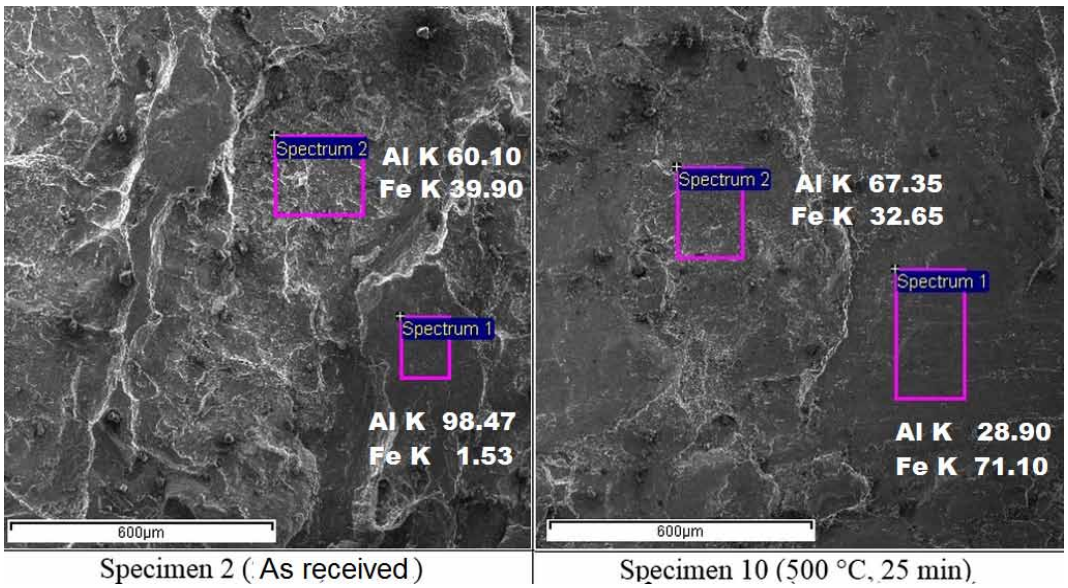

Fig. 11. SEM-EDS elemental analysis (at.-%) of black (Spectrum 1) and white (Spectrum 2) regions at the fractured surfaces of specimen 2 and 10

the black region, as seen from the side view of specimen 10, similarly in ref. [22]. Therefore, the specimen 10 has more white areas and flat fracture surface compared to specimen 5, having a heat treatment at 300°C for 25 min.

It is clear that fragile intermetallic phases, which appear as a white color in SEM pictures, grow between AA1050 aluminum-steel interfaces and weaken the bonding to decrease the strength of the joint with increasing temperature of the heat treatment. This decrease is similar to the findings in ref. [10]. The fracture surface of the thermally loaded specimen 10 shows nearly 0% plastic deformation, as can be seen in Fig. 10. At the same time, surface roughness decreased by the growth of the intermetallic

phase, which was an evidence of brittle fracture. This is also in agreement with the findings in ref. [10], but differently, it is stated that the intermetallic layer thickens. It is seen in Fig. 9 that the black colored ductile fracture surface was observed when the intermediate aluminum layer was deformed.

Hardness values of specimen 2, 5, and 10 are given in Table 5. The location designations are shown in Fig. 1. Location C represents the interface section of the STJ. Therefore, this point was investigated to understand the effects of temperature and duration on the hardness of the specimens. For specimen 2 (as received), the hardness of the intermetallic phase is 220.8 HV, and for specimen 10 (500°C, 25 min.), it increased to 280 HV, which was a proof of more brittle phase formation depending on time and temperature.

Mechanical strength is enhanced by a wavy melted front layer that cleans the oxide layer from the surface during explosive welding, and thus larger bonding area is produced between joint interfaces. The strength values of the specimens decrease with the increasing temperature, and mechanical behavior changes from ductile to brittle since specimens fail with less displacement, which can be observed from Fig. 12.

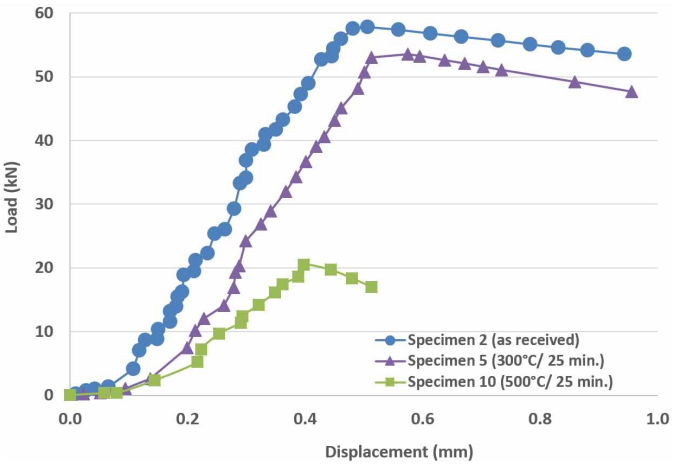

Fig. 12. Load displacement curve of specimens 2, 5, and 10

4. Conclusion

In this experimental study, ram tensile tests, micro-hardness tests, and microstructural examinations were performed on the aluminum/steel STJ made from shipbuilding D Grade Steel, 5083 series aluminum, and 1050 series aluminum as an intermediate layer. The hardness of the aluminum/steel interface increased from 220 HV to 280 HV with heat treatment, and the cause of a decrease in bonding strength is explained by the growth of brittle phases. The toughness decreased due to brittle fracture that can also be seen as a reduction of the area under the load-displacement curve in Fig. 12. Heat treatment at 500°C with more than 15 minutes duration, the tensile strength of the studied material is under the minimum requirement of MIL-J-24445A standard (75 MPa). If the STJ is subjected to more severe conditions, its mechanical behavior changes from ductile to brittle fracture due to the intermetallic layer that enlarges and covers the entire layer between the steel and aluminum bonding surface.

Acknowledgment

This study was presented as a part of the MSc. thesis of the second author.

REFERENCES

[1] G. Costanza, V. Crupi, E. Guglielmino, A. Sili, M.E. Tata, Metall. Ital. **11**, 17-22 (2016).
[2] L. Shao, Y. Shi, J.K. Huang, S.J. Wu, Mater. Design **66**, 453-458 (2015).
[3] G. Zhang, M. Chen, Y. Shi, J. Huanga, F. Yang, Rsc. Adv. **7**, 37797-37805 (2017).
[4] Q.M. Nguyen, S.C. Huang, Materials **8**, 8246-8254 (2015).
[5] W. Liu, J. Ma, M.M. Atabaki, R. Kovacevic, Mater. Design **68**, 146-157 (2015).
[6] J. Sun, Q. Yan, W. Gao, J. Huang, Mater. Design **83**, 120-128 (2015).
[7] S. Meco, L. Cozzolino, S. Ganguly, S. Williams, N. McPherson, J. Mater. Process Tech. **247**, 121-133 (2017).
[8] L. Tricarico, R. Spina, Mater. Design **31**, 1981-1992 (2010).
[9] S. Phengsakula, A. Rodchanarowana, Energy Proced. **34**, 782-790 (2013).
[10] L. Tricarico, R. Spina, Arch. Mater. Sci. Eng. **37**, 85-93 (2009).
[11] L. Tricarico, R. Spina, D. Sorgente, M. Brandizzi, Mater. Design **31** (7), 2693-2700 (2009).
[12] S. Xian-jun, T. Jie, G. Xun-Zhong, T. Nonferr. Metal. Soc. **21**, 2175-2180 (2009).
[13] H. Paul, M. Faryna, M. Prazmowski, R. Banski, Arch. Metall. Mater. **56** (2), 463-474 (2011).
[14] H. Paul, M.M. Miszczyk, A. Gałka, R. Chulist, Z. Szulc, Arch. Metall. Mater. **64** (2), 683-694 (2019).
[15] J. Hasenclever, in: J.F. Nie, A.J. Morton, B.C. Muddle (Ed.), Recrystallisation and Texture, The Institute of Materials Engineering Australasia Ltd, Melbourne (2004).
[16] N. Jimenez-Mena, A. Simar, P.J. Jacques, Mater. Design **180** (10795), 1-11 (2019).
[17] M.K.G. Shiran, H. Bakhtiari, S.A. Mousavi, G. Khalaj, S.M. Mirhashemi, Materials Research **20** (2), 291-302 (2017).
[18] L. Agudo, D. Eyidi, C.H. Schmaranzer, E. Arenholz, N. Jank, J. Bruckner, A.R. Pyzalla, Journal of Material Science **42**, 4205-4214 (2007).
[19] H. Springer, A. Szczepaniak, D. Raabe, Acta Materialia **96**, 203-211 (2015).
[20] P. Matysik, S. Jóźwiak, T. Czujko, Materials **8**, 914-931 (2015).
[21] M. Mhedhbi, M. Khlif, C. Bradai, Journal of Materials and Environmental Sciences **8**, 2967-2974 (2017)
[22] M Yildirim, Ph.D. Thesis, Design and Development of Iron Aluminium Intermetallic Compounds For Structural Applicatıons at High Temperatures, Middle East Technical University, Ankara, Turkey (2014).